ACS OMEGA

http://pubs.acs.org/journal/acsodf

Article

# Synthesis and Computational Study of an Optical Fluorescent Sensor for Selective Detection of $Ni^{2+}$ Ions

Maria Sadia, Jehangir Khan, Rizwan Khan, Syed Wadood Ali Shah, Adil Zada, Muhammad Zahoor,* Riaz Ullah, and Essam A. Ali

Cite This: *ACS Omega* 2023, 8, 27500−27509

Read Online

ACCESS | Metrics & More | Article Recommendations | Supporting Information

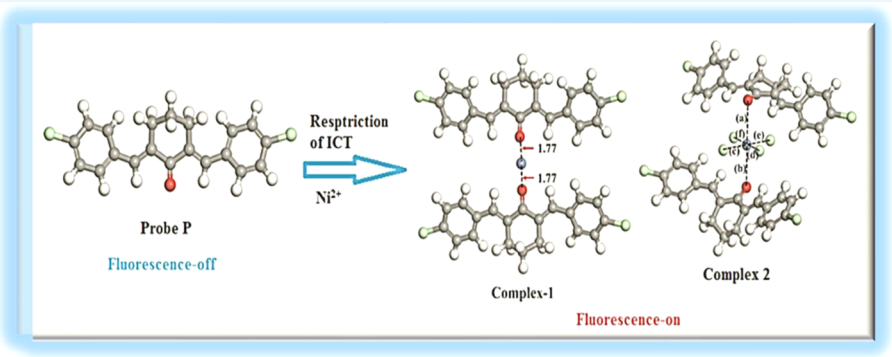


**ABSTRACT:** The presence of an abnormal amount of $Ni^{2+}$ in the human body causes various health issues. Therefore, this work aimed to synthesize the curcumin-based fluorescence-on sensor ***P*** [2,6-bis((*E*)-4-chlorobenzylidene)-cyclohexan-1-one] that was capable of selectively responding to $Ni^{2+}$ ions in aqueous solution. The structure of ***P*** was confirmed by $^1$H NMR and Fourier transform infrared (FTIR) spectroscopy. The $Ni^{2+}$ ion sensing was based on the fluorescence enhancement of the fluorophore (***P***) in neutral aqueous medium. The response of the ***P***-based sensor was highly selective toward $Ni^{2+}$ ions, whereas the possible interferences from other metal cations were negligible. ***P*** had a fast response; it was selective and had a sensitive detection limit (LOD = $2 \times 10^{-10}$ M) toward $Ni^{2+}$ ions in neutral medium with a high association constant ($K$) value of $3.6 \times 10^5$ $M^{-2}$ for the complex formation between the ***P*** and $Ni^{2+}$ ions. Job's plot and DFT calculations proved that the binding stoichiometry of ***P*** for $Ni^{2+}$ was 2:1. ***P*** was recovered using EDTA as a chelating agent after being employed as a fluorescent sensor. These characteristics ensured the potential use of ***P*** as a new class of chemosensor for environmental applications.

## 1. INTRODUCTION

Worldwide, water pollution has become a serious problem with rapidly increasing industrialization.[1] Environmental pollution is one of the major challenges in modern human society.[2] Environmental contamination and pollution by heavy metals are a threat and of serious concern to the environment.[3] Industrial effluents as well as domestic sewage are continuously discharged into water bodies, which mostly contain heavy metal ions.[4] Due to their coordination ability, heavy metal ions are highly toxic, thereby directly or indirectly affecting the environment and human health. The $Ni^{2+}$ ion, in particular, is highly hazardous for human and marine life even at low concentrations.[5] The World Health Organization (2000) recommended the maximum permissible limit for $Ni^{2+}$ ions in drinking water up to 0.02 mg $L^{-1}$.[6] $Ni^{2+}$ ions are stable and accumulate in the environment and organism bodies for a longer period. Depending on the dose and length of exposure, nickel causes different effects in organisms. Hence, time demands the development of materials for fast and selective removal of $Ni^{2+}$ ions from water samples. Various methods have been developed for the removal of $Ni^{2+}$ ions from aqueous samples, including atomic absorption spectroscopy,[7] liquid−liquid extraction,[8] co-precipitation,[9] solid-phase extraction,[10] inductively coupled plasma mass spectrometry,[11] and electrochemical deposition.[12] Although these methods exhibit good sensitivity and selectivity, yet their applications are limited due to their high operational cost, nonportability of instruments, sophisticated sample preparation, and need of intense technical training. Thus, the development of simple, rapid, sensitive, and less expensive methods is highly demanded. Fluorescence-based detection of $Ni^{2+}$ ions gained the attention of the scientific community due to its simplicity,

**Received:** May 6, 2023
**Accepted:** July 7, 2023
**Published:** July 19, 2023





https://doi.org/10.1021/acsomega.3c03131
*ACS Omega* 2023, 8, 27500−27509

low cost, quick response, and environmentally friendly nature.[13] However, the fluorescence-based sensor has some limitations including low sensitivity, lack of selectivity, poor solubility of the probe, and serious interference by other metals. To overcome these shortcomings, organic probe-based fluorescent sensors have been reported, which show better fluorescence sensing of $Ni^{2+}$.[14] An efficient fluorescence performance is shown by these organic probes for the detection of $Ni^{2+}$ due to the presence of good optical properties and high solubility and stability. Also, these probes are found to be more suitable for making complexes with divalent metal ions such as $Ni^{2+}$ via restricting ICT phenomena. Furthermore, at specific excitation and emission wavelengths, complexes with metal ions also enhance the optical behavior. The signals from emission and absorption changes of light by fluorophores provide information about the mechanism of sensing of $Ni^{2+}$ ions. Goswami et al.,[15] Sarkar et al.,[16] Prabhu et al.,[17] Biswajit Chowdhury et al.,[18] and Santhi et al.[19] have developed organic probe-based fluorescent sensors for the detection of $Ni^{2+}$ in aqueous medium. However, the sensitivity and selectivity of this organic probe-based fluorescence are still not ideal. Therefore, in this work, we have focused on the synthesis of a curcumin derivative (***P***)-based fluorescence-on sensor that could detect $Ni^{2+}$ with selectivity and sensitivity in aqueous medium. Due to the presence of best coordination sites, ***P*** was capable of forming stable complexes with $Ni^{2+}$ ions. The sensing mechanism of ***P*** was based on competitive binding with $Ni^{2+}$ ions among different metal ions.

## 2. EXPERIMENTAL SECTION

**2.1. Chemicals and Instruments.** Cyclohexanone (Sigma Aldrich), 4-dimethyl aminobenzaldehyde (Alfa Aesar), NaOH (Merck), and all metal salts (BDH chemicals England) in the form of chloride or nitrate including $Cd(NO_3)_2{\cdot}4H_2O$, $Hg(NO_3)_2$, $Co(NO_3)_2{\cdot}4H_2O$, $Ce(NO_3)_3{\cdot}6H_2O$, $Zn(NO_3)_2{\cdot}6H_2O$, $CuCl_2{\cdot}2H_2O$, $Mn(NO_3)_2{\cdot}4H_2O$, $NiCl_2{\cdot}6H_2O$, $Cr(NO_3)_3$, and $Pb(NO_3)_3$ were used. All the chemicals were used without any further purification. Solution pH was measured with a digital pH meter (Merck). For fluorescence and absorption spectral measurements, a spectrophotofluorometer RF-5301 PC (Shimadzu, Japan) and 1601 Double-beam UV−visible Spectrophotometer (Tokyo, Japan) was used. $^1$H-NMR and FTIR spectra were taken on a Bruker Avance 400 MHz spectrometer (Varian) and FTIR instrument Prestige 21 (Shimadzu, Japan) in the 400−4000 $cm^{-1}$ range, respectively. All chemical shifts were recorded on the $\delta$-scale in deuterated chloroform ($CDCl_3$) solvent.

**2.2. Synthesis of [2,6-Bis(*E*)-4- chlorobenzylidene-cyclohexan-1-one] *P*.** [2,6-Bis((*E*)-4-chlorobenzylidene)-cyclohexan-1-one] was synthesized by reacting 4-chlorobenzaldehyde at 12 mmol (1.68 g), in 15 mL of ethanol and 6 mmol (0.58 g) cyclohexanone. Then, 10 mL of sodium hydroxide (10%) was added to the reaction mixture in a dropwise manner. The mixture was refluxed for 4 h; the thin-layer chromatographic technique was used for determining the reaction progress. The final product was processed in ice, with the addition of the HCl/water (30:70) mixture, resulting in yellow color crystals having *M*p 158−159 °C. $^1$H-NMR: $\delta$ 7.74 (s, 2H═CH), 7.40 (m, 8H, ArH), 2.91 (m, 4H, $2CH_2$), 1.82 (m, 2H, $CH_2$), 1.82 (m, 2H, $CH_2$). The IR (KBr) spectrum ($\nu$ $cm^{-1}$): 1628−1649 (C═C Ar), 2997−2935 (C−H asymmetric), 1713 (C═O) 3027, (C−H Ar).

**2.3. Spectroscopic Studies.** UV−visible and fluorescence spectroscopic analyses were used for exploring the optical properties and metal ion detecting capability. In all experiments, ***P*** and metal ion solutions (stock and working) were prepared in acetonitrile and distilled water, respectively. The concentration of the stock solution was 0.01 mM, and that of the working solution was 12 $\mu$M ***P***. The metal solution was 0.0.1 mM stock, and the working solution was 18 $\mu$M in all experiments except in initial fluorescence studies. The wavelength of excitation and emission was 330 and 580 nm, respectively. Excitation and emission spectra of probe ***P*** and its $Ni^{2+}$ complex are shown in Figure S2. The UV−visible spectrum of ***P*** (12 $\mu$M) separately in acetonitrile and its complex with nickel (II) ions (18 $\mu$M) in distilled water was recorded.

**2.4. Selection of a Suitable Solvent.** In the current study, acetonitrile was used as a solvent for ***P*** as acetonitrile offers excellent chemical stability, ensuring reliable experimental conditions. Also, it has excellent solubility properties, ensuring the effective dissolution of the probe. This choice allowed for the creation of a homogeneous solution, which was crucial for accurate and reliable measurements.

**2.5. Effect of Time on Fluorescence Intensity.** The time study on fluorescence intensity was assayed for both ***P*** (12 $\mu$M) and its $Ni^{2+}$ ion (18 $\mu$M) complex. The fluorescence spectra were recorded in the 5−50 min range.

**2.6. Detection and Quantification Limit.** The detection and quantification limits were determined using eqs 1 and 2, respectively

$$LOD = \frac{3\delta}{S} \tag{1}$$

$$LOQ = 3.\ \mathrm{LOD} \tag{2}$$

where "$\delta$" is the standard deviation and "*S*" is the slope of fluorescence vs sample concentration curve.

**2.7. Computational Details.** The computational intentions were carried out with the sub-density functional theory (DFT) flavor Becke's Lee−Yang−Parr's correlation function (B3LYP),[20] Gaussian-09 code.[21] The empirical dispersion GD3[22] was used to accurately describe empirical dispersion correction in the intermolecular interactions during the complexation. For the rest of the computations, the 6-31G(d,p)[23] basis set was used. The frequency calculations were employed to ensure whether the geometries correspond to potential energy minima or not. The imaginary frequency absence confirmed that all the geometries correspond to potential energy minima. To evaluate the binding energy ($E_{bind}$), eq 3[24] was used.

$$E_{bind} = E_{complex} - (E_{probe} + Ni^{2+}) \tag{3}$$

where $C_{omplex}$ is the total energy of the complex (***P*** and nickel ion) and $E_{probe}$ and $E_{Ni}{}^{2+}$ are the total energy of probe ***P*** and Ni ion, respectively.

**2.8. Fluorogenic Recognition of Nickel(II) Ions in Aqueous Samples and Reusability Study.** The effectiveness of ***P*** toward nickel(II) ion detection was evaluated in different aqueous samples. For this purpose, river, tap, and lake water samples were collected, filtered, and stored in polyethylene bottles. Spiking was performed in a concentration range of nickel(II) ions (2−18 $\mu$M) at constant (12 $\mu$M) ***P***. The reusability experiments were performed using ethylenedi-



https://doi.org/10.1021/acsomega.3c03131
ACS Omega 2023, 8, 27500−27509

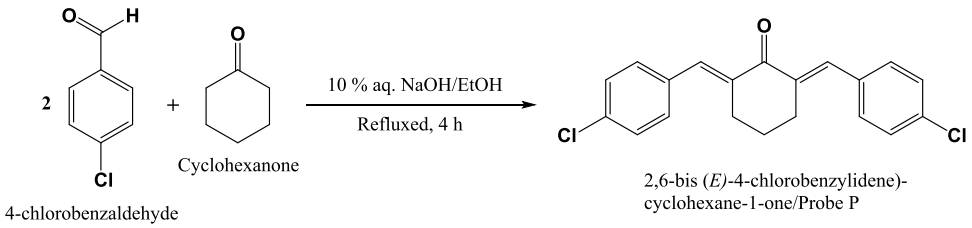


**Figure 1.** Schematic representation of the synthesis of probe ***P*** through aldol condensation.

amine tetra acetic acid (EDTA) as a reversibility agent. The concentration of EDTA and $Ni^{2+}$ used was 18 $\mu$M.

**2.9. EDTA as a Chelating Agent for the Reversibility Experiment.** A number of chelating agents can be used as reversibility agents such as diethylenetriaminepentaacetic acid (DTPA), *N*,*N*0-bis-(dithiocarboxy)piperazine, nitrilotriacetic acid (NTA), and 1,3,5-hexahydrotriazinedithiocarbamate. However, among these chelating agents, EDTA was used for reversibility studies due to its easy availability, low cost, and no interference with results.

## 3. RESULTS AND DISCUSSION

**3.1. Synthesis and Characterization.** ***P***/[2,6-Bis((*E*)-4-chlorobenzylidene)-cyclohexan-1-one] was synthesized by the base-catalyzed reaction between 4-chlorobenzaldehyde and cyclohexanone with 74% yield (Figure 1).

The functional groups of the synthesized ***P*** were confirmed by FT-IR spectroscopy (Figure 2). The peaks at 1628−1649

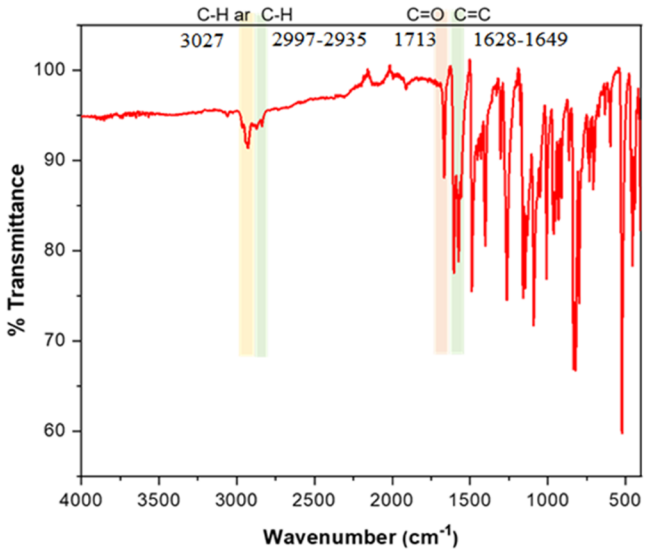


**Figure 2.** Fourier transform infrared spectroscopic analysis of ***P***.

and 2997−2935 $cm^{-1}$ were attributed to C═C aromatic and C−H vibration, respectively. The absorption peak around 1713 $cm^{-1}$ indicated the presence of the C═O group, and the peak at 3027 $cm^{-1}$ represented the existence of C−H aromatic vibrations.[25]

The proton NMR spectrum of ***P*** showed distinctive peaks around $\delta$ 7.74 and 7.40 demonstrating the presence of 2H═CH and Ar protons. The signals at 2.91 and 1.82 were attributed to 4H and methylene protons, respectively (Figure S1).

**3.2. Preliminary Study.** Initially, the UV−visible spectra of ***P*** and the probe ***P***−nickel(II) ion complex were measured in a wide range of wavelengths (260−400). The spectrum of ***P*** exhibited maximum absorption at around 300 nm and would shift to 330 nm upon the addition of $Ni^{2+}$ ion solution, revealing the complexation of ***P*** with $Ni^{2+}$ ions. Significant enhancement in absorption wavelength was observed after the complexation of **P** with $Ni^{2+}$ ions (Figure 3a). The complexation study of ***P*** with different metal ions was recorded by fluorescence spectroscopy. The fluorescence spectra of ***P*** showed an emission band at 580 nm in acetonitrile (12 $\mu$M). Among the addition of various metal ion solutions (220 $\mu$M in $H_2O$), the emission band at 580 nm underwent significant enhancement with $Ni^{2+}$ in comparison with other metal ions (Figure 3b,c). The $Ni^{2+}$ ion sensing was based on the fluorescence enhancement of the fluorophore (***P***) in neutral aqueous medium.[26] The probe in the absence of $Ni^{2+}$ exhibited a pale yellow color, while after making complex with $Ni^{2+}$, a visible color change was observed from pale yellow to deep yellow color. For the complexes of P with other metal ions, a slight color change was observed, indicating poor complex formation. These results indicated a high affinity of ***P*** in terms of fluorescence intensity toward the $Ni^{2+}$ ion; therefore, based on these initial results, further fluorescence analyses were performed. The visual color change of free probe P and its $Ni^{2+}$ complex and complexes with other metal ions is shown in Figure 4.

**3.3. Effect of Time.** The fluorescence response by a change in time of ***P*** toward $Ni^{2+}$ ions was studied by taking probe ***P*** (12 $\mu$M) separately and then its complex with the $Ni^{2+}$ ion (18 $\mu$M) and recording fluorescence spectra in the range of 5−50 min, at 580 nm. As shown in Figure 8b, for both probe ***P*** and ***P***-$Ni^{2+}$, the intensity remained constant, indicating the stability of the complex.[27]

**3.4. Effect of the $Ni^{2+}$ Ion Concentration.** The fluorescence titration studies showed that a linear enhancement in fluorescence was observed with increasing $Ni^{2+}$ concentration from 2 to 18 $\mu$M at constant ***P*** (12 $\mu$M) as shown in Figure 6a. The detection limit was calculated from Figure 6a using eq 1. The limits of detection and quantification were $2.0 \times 10^{-10}$ and $6.0 \times 10^{-10}$ M, respectively. Similarly, UV−vis absorption titration was also performed and is shown in Figure 5b. The fluorescence emission spectra of ***P*** (12 $\mu$M) complexes with incremental concentration of $Ni^{2+}$ (2−18 $\mu$M) were recorded as shown in Figure 8c. The results showed that the fluorescence intensity increased up to 18 $\mu$M.

**3.5. Binding Stoichiometry and Association Constant Determination.** For the current study (10 $\mu$M), solutions of both ***P*** and $Ni^{2+}$ were prepared for Job's plot analysis. For the experiment, the ***P*** (0.1−0.9) molar concentration range was used. Throughout the experiment, the total concentrations of ***P*** and $Ni^{2+}$ ions were kept constant. Maximum fluorescence intensity was observed at 0.6 mole fraction of ***P*** as shown in (Figure 5a), indicating a 2:1 ratio between ***P*** and $Ni^{2+}$ ion. The photophysical properties of probe ***P*** are shown in Table 1. The


https://doi.org/10.1021/acsomega.3c03131
ACS Omega 2023, 8, 27500−27509

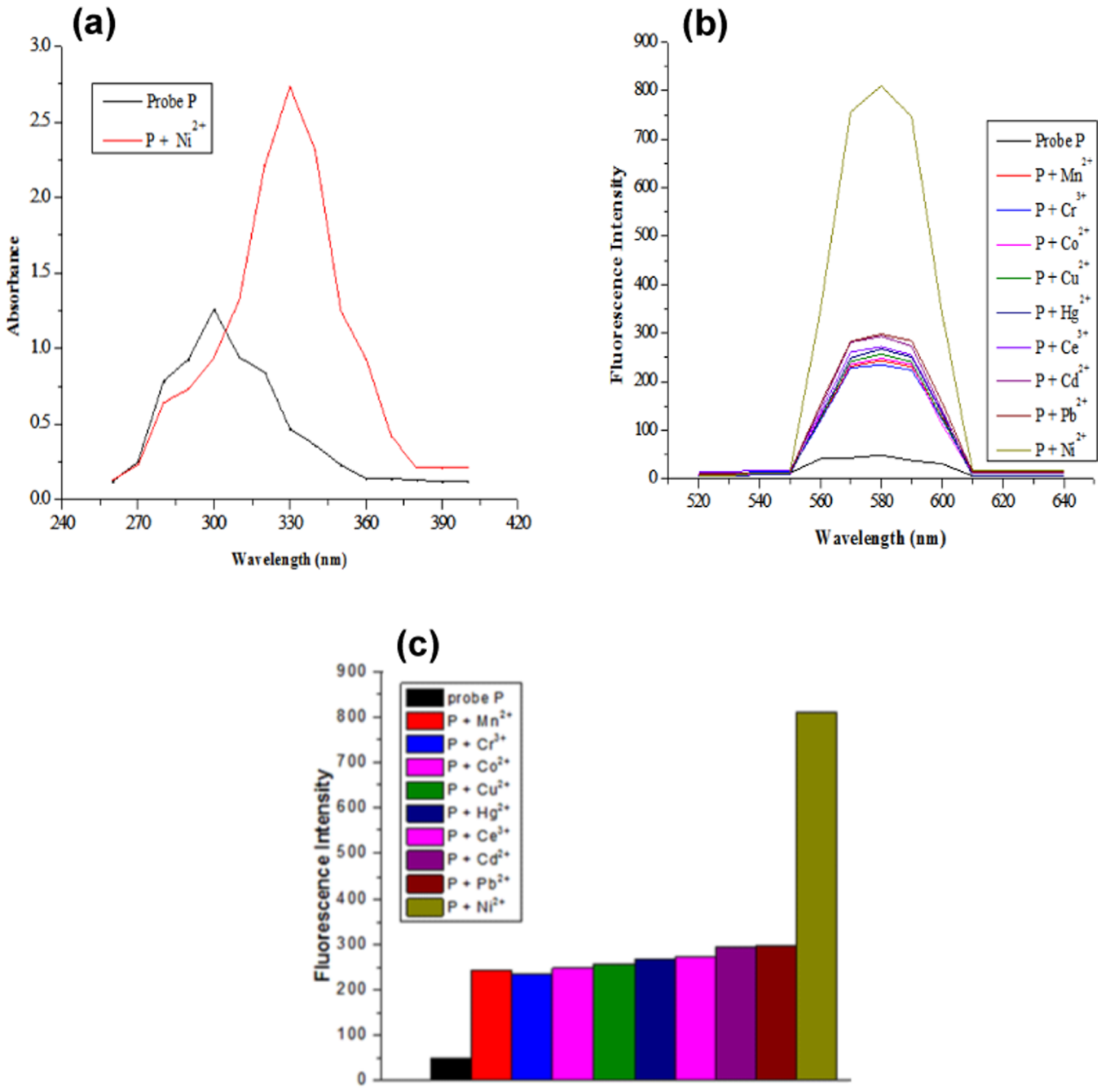


**Figure 3.** (a) UV−vis absorption study of ***P*** and ***P***−nickel(II) complex, using ***P*** = (12 $\mu$M) and $Ni^{2+}$ ion = (18 $\mu$M); (b) preliminary study of ***P*** (12 $\mu$M) and metal ions (220 $\mu$M) at $\lambda_{ex}/\lambda_{em}$ = 330:580 nm; and (c) representation of preliminary study by a bar graph for clarity.

association constant ($K_a$) was $3.6 \times 10^5$ $M^{-2}$, calculated from the Benesi−Hilderbrand plot (Figure 6b). The association constant of ***P*** is higher than that of the previously reported organic probe-based fluorescence sensors, thus confirming the good binding capability of ***P*** toward $Ni^{2+}$ ions.

The accuracy of the stability constant determination does not depend solely on the concentration of one of the reagents; it is essential to have accurate measurements of all reagents involved in the reaction to obtain a precise determination of the stability constant. If the concentration of one of the reagents cannot be measured precisely, Job's plot can still be used as a graphical method to determine the stoichiometry of the metal−ligand complex. However, the accuracy of the stability constant determination using Job's plot may be limited due to the binding stoichiometry and the effects of competing reactions or solution conditions that may affect the absorbance measurements.

Therefore, the accurate measurement of the concentration of all reagents involved in the reaction is crucial to obtain a precise determination of the stability constant, and Job's plot should only be used as a complementary method when the exact concentrations of the reagents are unknown or difficult to measure accurately.

**3.6. Mechanism of $Ni^{2+}$ Detection.** In the current study, the free probe ***P*** showed quenching in fluorescence intensity due to ICT phenomena, while after binding with $Ni^{2+}$, the ICT phenomena were restricted and hence, fluorescence intensity enhanced. The chelation of Ni(II) with the carbonyl group in


https://doi.org/10.1021/acsomega.3c03131
ACS Omega 2023, 8, 27500−27509

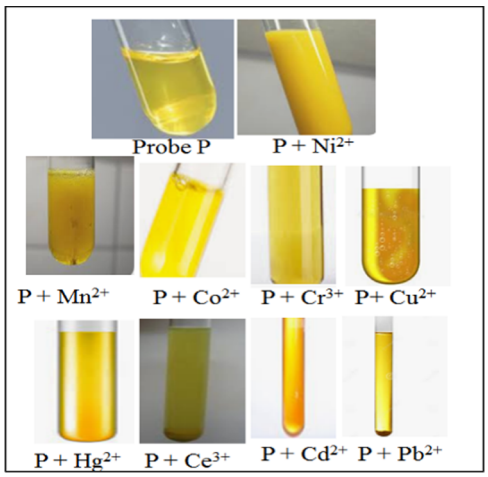


**Figure 4.** UV−visible color change of probe ***P*** and its complex with $Ni^{2+}$ and other metal ions.

our probe generated a coordination complex that exhibited different electronic characteristics compared to the free ligand. The presence of Ni(II) could have modified the energy levels and electronic transitions within the system, resulting in a bathochromic shift toward longer wavelengths in the UV range. This shift is commonly observed when metal−ligand interactions occur. Additionally, chelation with Ni(II) enhanced the fluorescence emission of the probe. The coordination of the metal ion stabilized the excited state of the fluorophore, reducing nonradiative decay pathways and increasing the fluorescence quantum yield. This phenomenon is often observed in chelation-based fluorescent probes. The Ni(II)-mediated turn-on fluorescence of probe ***P*** was based on the ligand's electronic properties, enabling efficient charge transfer from the ligand to the Ni(II) ion upon excitation. This charge transfer process resulted in enhanced fluorescence emission compared to the free ligand. The coordination of the ligand with Ni(II) created a favorable environment for ligand-to-metal charge transfer (LMCT), leading to an increased excited-state population and higher fluorescence intensity in the presence of Ni(II) ions.

**3.7. Sensitivity and Selectivity of Probe *P* toward $Ni^{2+}$ Ions.** The next experiment was performed to investigate the selectivity of ***P*** toward $Ni^{2+}$ by the addition of other metal ions (manganese(II), copper(II), cobalt(II), chromium(III), cerium(III), zinc(II), cadmium(II), lead(II), and mercury(II)). For this purpose, the fluorescence performance of the probe complex with $Ni^{2+}$ in the presence of the above-mentioned interfering metal ions was recorded. The results showed that even in the presence of a higher concentration of these co-existing metal ions, the fluorescence intensity remained constant, indicating the high selectivity of ***P*** for $Ni^{2+}$ ions (Figure 6c,d).

A best sensor is one that shows minimum interference for the target metal ions from other available metal ions. The selectivity of the probe for making a selective complex with $Ni^{2+}$ was also confirmed by taking replicate analysis. Furthermore, the high selectivity of the current probe for detecting $Ni^{2+}$ can be attributed to several logical factors. First, ***P*** possesses a specific carbonyl functional group that is known to exhibit strong binding affinity toward $Ni^{2+}$ ions. This functional group allowed for specific recognition and binding of $Ni^{2+}$ ions, while potentially minimizing interactions with other metal ions. Even if the carbonyl group is capable of binding with Ni(II), it does not necessarily imply that the probe will exhibit the same response to other positively charged metal ions, such as Al(III) and Fe(III). Different metal ions have distinct coordination preferences and affinities for ligands. While the carbonyl group may form coordination bonds with Ni(II), it may not interact favorably or selectively with other metal ions due to differences in their electronic configurations and coordination geometries. Therefore, the probe's response to metal ions other than Ni(II) cannot be solely extrapolated based on the presence of a carbonyl group. We did measure the emission of the compound with all tested metal ions, but Ni(II) with the ligand showed a significant increase in emission as compared to other metal ions. The significant increase in emission observed with Ni(II) can be attributed to favorable ligand-to-metal charge transfer (LMCT) transitions and the stabilization of excited states. These factors resulted in a more pronounced enhancement of emission for Ni(II) compared to other tested metal ions. However, the extent of emission enhancement with other

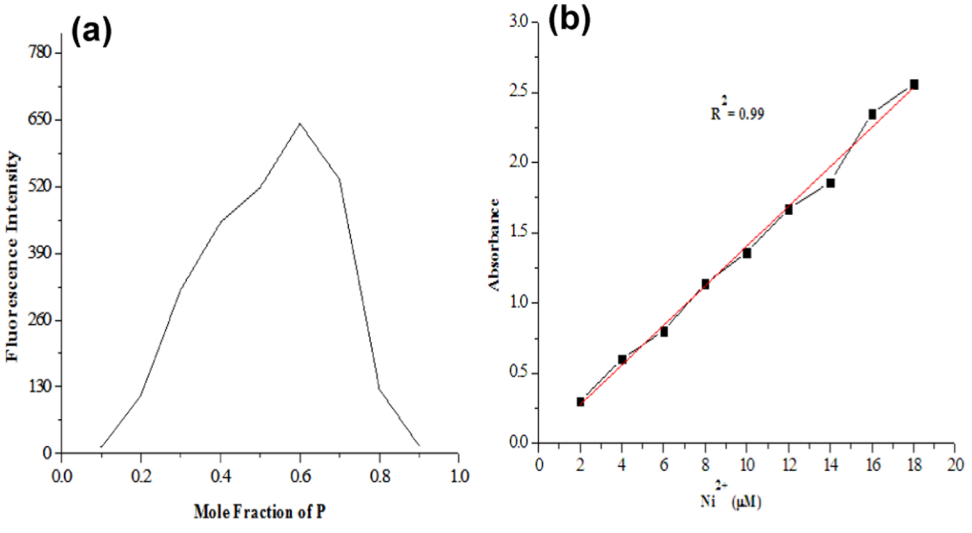


**Figure 5.** (a) Binding stoichiometric analysis (b). Absorption titration study in ***P*** (12$\mu$M) and $Ni^{2+}$ (2−18$\mu$M).



https://doi.org/10.1021/acsomega.3c03131
ACS Omega 2023, 8, 27500−27509

**Table 1. Photophysical Properties of *P***

| $\lambda_{ex}$ (nm) | $\lambda_{em}$ (nm) | association constant ($M^{2-}$) | LOD (M) | LOQ (M) | standard deviation | color of ***P*** |
|---|---|---|---|---|---|---|
| 330 | 580 | $3.6 \times 10^5$ | $2.0 \times 10^{-10}$ | $6 \times 10^{-10}$ | 0.75 | pale yellow |

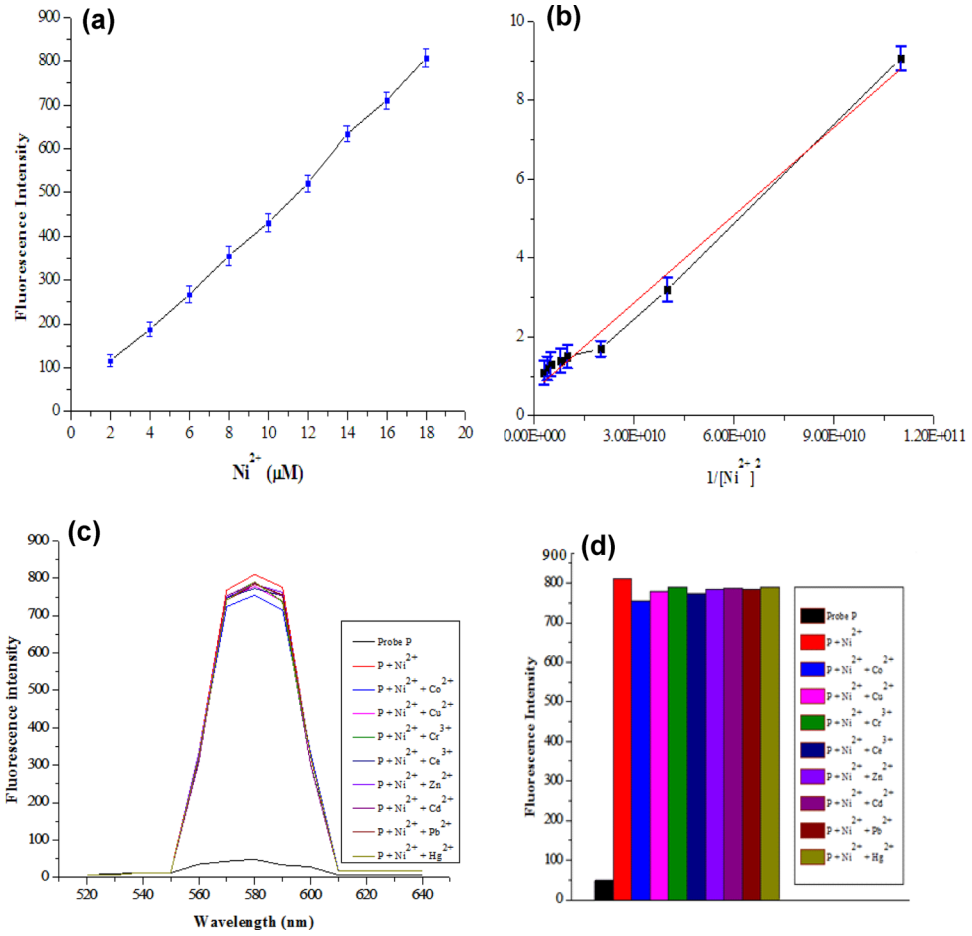


**Figure 6.** (a) Effect of $Ni^{2+}$ ion concentration (2−18 $\mu$M), ***P*** = (12 $\mu$M), and $\lambda_{em}$ = 580 nm; (b) Benesi−Hilderbrand plot analysis of probe ***P***; (c) interference study of the ***P***−nickel(II) complex in the presence of a higher concentration of interfering metal ions, $\lambda_{em}$ = 580 nm; and (d) representation of the interference study by a bar graph for clarity.

metal ions was lower due to differences in their coordination preferences, electronic properties, and overall binding affinities. These variations in metal ion-specific interactions affect the efficiency of energy transfer processes and subsequent emission enhancement.

Furthermore, the size compatibility between the ***P*** and the $Ni^{2+}$ ion played a crucial role in its selectivity. The ***P*** was designed to have dimensions and structural features that aligned well with the size and coordination preferences of $Ni^{2+}$. This enabled the probe to form stable complexes with $Ni^{2+}$ ions, while potentially hindering interactions with ions of different sizes. Additionally, the binding nature of ***P*** and $Ni^{2+}$ ions contributed to its selectivity. The probe underwent specific coordination interactions, such as chelation or coordination through lone pairs of electrons, which are particularly favorable for $Ni^{2+}$. This binding nature enhanced the selectivity of the probe toward $Ni^{2+}$ ions, as it ensured strong and specific interactions, while potentially reducing binding affinity toward other metal ions that lack similar coordination preferences.

**3.8. DFT Calculation.** The absorption and fluorescence analysis showed that almost every metal atom was capable of forming a complex with the ligand/probe ***P***. However, the highest enhancement was observed in the case of $Ni^{2+}$, indicating a high selectivity for this particular metal ion. Thus, we proceeded to investigate only the complexation reaction between the probe ***P*** and $Ni^{2+}$ through DFT calculations. Our experimental results were supported by the DFT calculations, which confirmed both the stability of the complex and the binding stoichiometry of 2:1 between the probe ***P*** and $Ni^{2+}$.

The bonding of atoms in a material is caused by the charged nature of the electron. Therefore, to understand the removal of $Ni^{2+}$ from water through an organic probe at the atomic level, the electronic properties of both the probe and metal ion must be studied. Density functional theory (DFT) is an effective tool that considers the quantum mechanical nature of electrons of a material.[28] The coordination site present in the probe is one carbonyl oxygen. The probe is to act as a monodentate. To gain full insights into the bonding strength between the active sites, i.e., O of the probe and $Ni^{2+}$ ion, we performed density functional theory (DFT) simulations. Nowadays, the DFT simulations are a powerful tool to predict correctly the bonding behaviors between the probe and $Ni^{2+}$ ion. In the present study, the DFT calculation was performed using the DMOL3


https://doi.org/10.1021/acsomega.3c03131
ACS Omega 2023, 8, 27500−27509

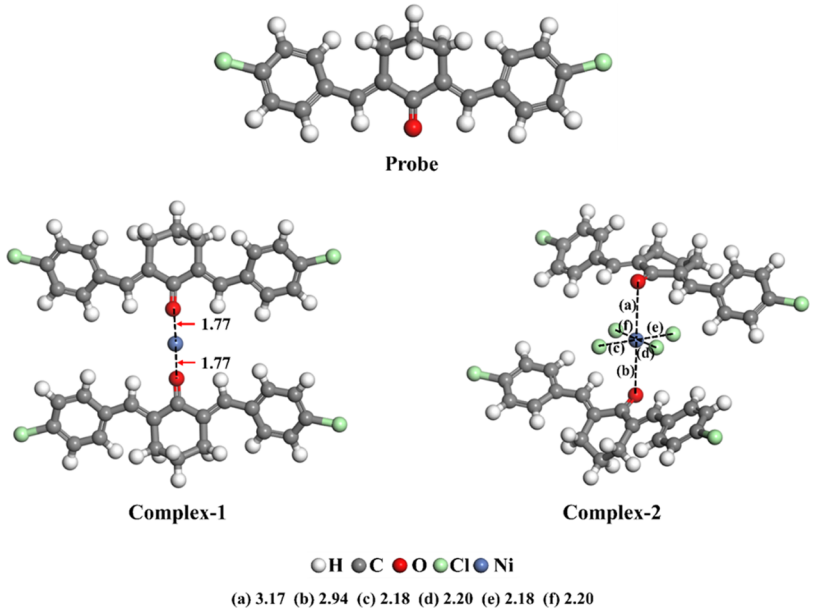


**Figure 7.** Optimized geometries of probe ***P*** and their complexes with $Ni^{2+}$ ions.

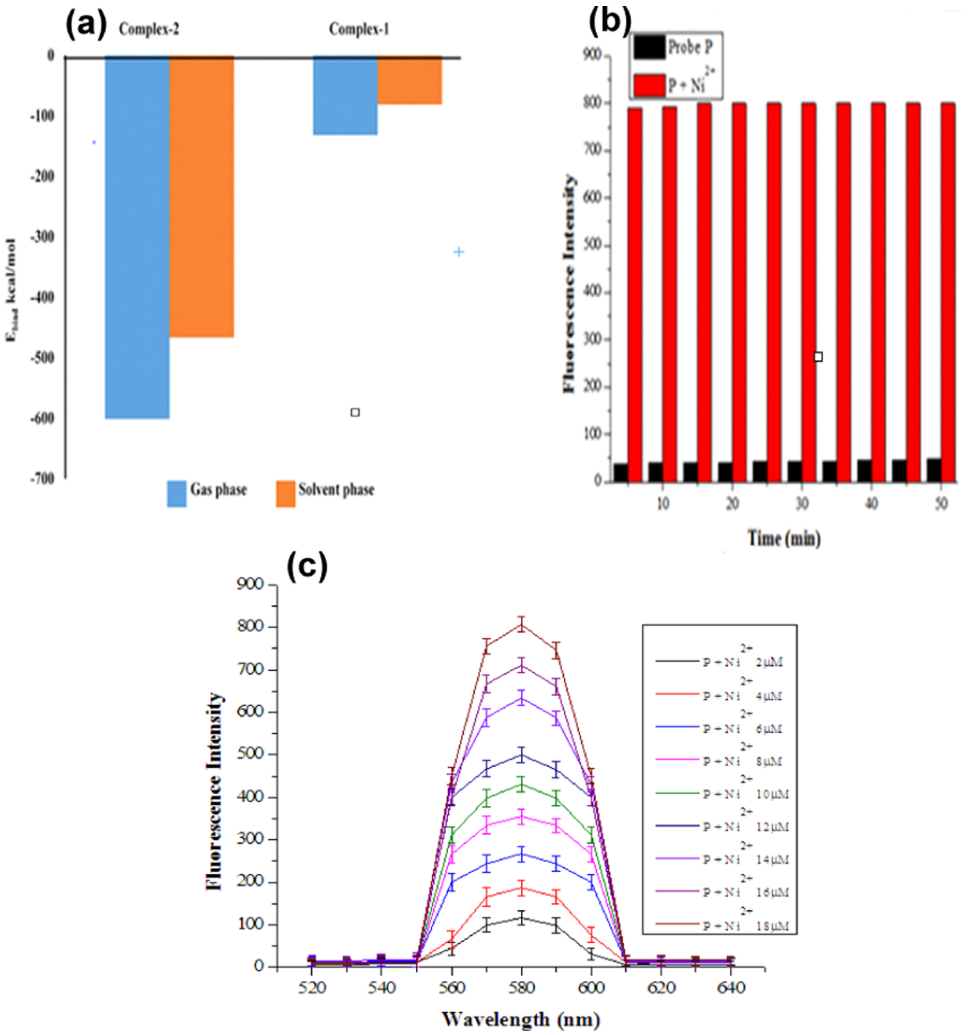


**Figure 8.** (a) Comparative energy profile of complexes of Ni(II) with ***P***. (b) Fluorescence response of ***P*** and ***P***-$Ni^{2+}$ in the range of 5−50 min at constant ***P*** and $Ni^{2+}$ concentrations. (c) Fluorescence spectra with increasing concentration of $Ni^{2+}$ (2−18 $\mu$M).



https://doi.org/10.1021/acsomega.3c03131
ACS Omega 2023, 8, 27500−27509

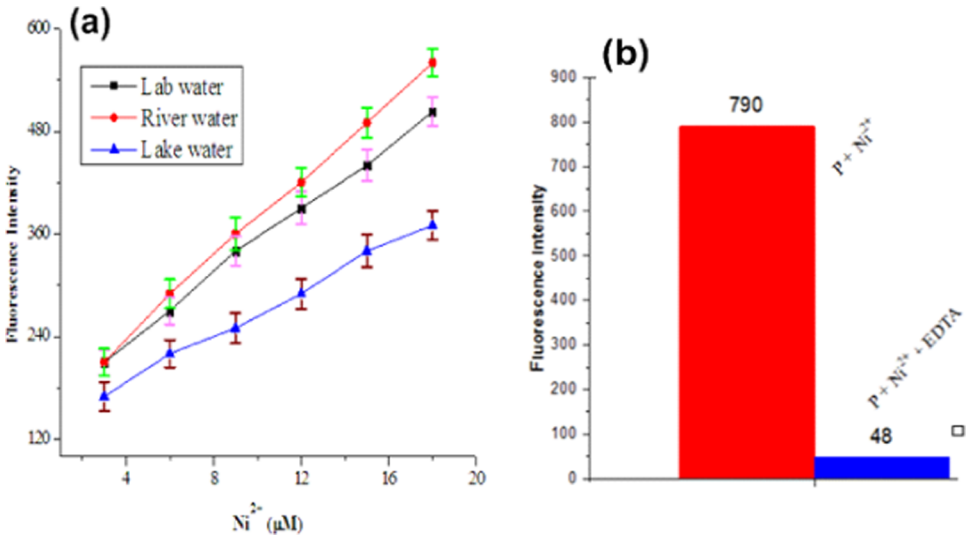


**Figure 9.** (a) Application of ***P*** (12 $\mu$M) in acetonitrile with $Ni^{2+}$ (18 $\mu$M) in distilled water, at $\lambda_{ex}$ = 330 nm and $\lambda_{em}$ = 580 nm. (b) Reusability of ***P***−nickel(II) employing EDTA as a chelating agent at $\lambda_{em}$ = 580 nm.

code,[29] Materials Studio. For the exchange-correlation function in these quantum chemical calculations, the Perdew−Burke−Ernzerhof (PBE) formulation was used within the generalized gradient approximation (GGA). The DFT + D2 method (Grimme's scheme) was applied for a long-range dispersion correction in intermolecular interactions. The double numerical plus polarization (DNP) basis set was employed for calculations, which was reliable in obtaining good results like Pople's 6-31G(d,p) basis set. Recently, the GGA/PBE method with the DNP basis set is frequently used for different complexation studies, which gives reliable results. The Fermi smearing was set to 0.005 Ha with a real space cutoff of 4.6 Å utilized in the calculations. The geometries of all the systems (monomers and complexes) were optimized at a convergence tolerance of $10^{-5}$ Ha, 0.002 Ha/Å, and 0.005 Å for the energy, force, and displacement, respectively.

Therefore, we performed a computational study for two different complexes as shown in Figure 7. In complex 1, the $Ni^{2+}$ interacts with the two carbonyl oxygen (C═O) of the ***P*** each at a distance of 1.77 Å, while in complex 2, the $Ni^{2+}$ interacts with the two carbonyl oxygen (C═O) of the probe and four chloride ion at a distance of 3.17 (a), 2.94 (b), 2.18 (c), 2.20 (d), 2.18 (e), and 2.20 Å (f), respectively.

The binding energies ($E_{bin}$) calculated (Table S1) using the same theory in gaseous and solvent phases for both complexes were found to be negative, which proved that the formation of these complexes was energetically favorable. The $E_{bin}$ (gas phase) for complex 1 (−733.86 kcal/mol) is more than that of complex 2 (−639.37 kcal/mol), indicating that complex 1 was more energetically favorable than complex 2. The order of $E_{bin}$ in the solvent (water) phase was similar to the gas phase, but the values were smaller than in the gas phase due to the greater value of the dielectric constant of water (78.5). Generally, by raising the dielectric constant of a medium, according to the Coulomb law, the force of attraction or repulsion between the charges decreases. The comparative graphical representation of both gas and solvent phases $E_{bin}$ is described in Figure 8a.

Furthermore, to check the nature of the interaction of $Ni^{2+}$ with ***P*** and $Cl^{-1}$, the difference in charge transfer ($\Delta q_{CT}$) was calculated by using Mulliken atomic charges. The obtained results indicated that after interaction of $Ni^{2+}$ with the probe and $Cl^{-1}$, a decrease was observed in the negative charges of oxygen atoms of the probe and $Cl^{-1}$. Similarly, a decrease in the positive charge of $Ni^{2+}$ ions was recorded. This illustrated that charge transfer occurred from the oxygen and chloride ions to the central metal ion, i.e., $Ni^{2+}$ ion.

**3.9. Environmental Sample Analysis and Reusability Test.** The analytical applicability of the prepared ***P*** is necessary to be evaluated. Therefore, ***P*** was applied to remediate the $Ni^{2+}$ ions from environmental water samples. For this purpose, different concentrations of $Ni^{2+}$ ions were spiked in tap, river, and lake water samples (Figure 9a). As can be seen from the results, ***P*** showed good results for the detection of $Ni^{2+}$ ions in these spiked water samples. The obtained results suggested that ***P*** is sensitive and reliable enough for the practical detection of $Ni^{2+}$ ions in environmental water samples. For a ***P*** to be economical and used at a large scale, its reusability should be high. The reversible fluorescence-based analysis is highly demanded in the modern period due to its wide applications. Therefore, to check the economic importance and efficiency of the prepared ***P***, it was subjected to reusability experiments. Ethylenediaminetetracetic acid (EDTA) was used as a reversible agent to investigate the reversible behavior of ***P***. Upon the addition of EDTA, the fluorescence intensity of the complex decreased (at $\lambda_{em}$ = 580 nm), which confirmed the recovery of ***P*** (Figure 9b). This result proved that ***P*** can be used reversibly for the detection of $Ni^{2+}$.

**3.10. Comparison of Probe *P* with the Reported Fluorescent Probes.** To check the practical advantage of the prepared ***P*** for $Ni^{2+}$ ion detection, the current work was compared with some other recently reported work based on detection and quantification limits as shown in Table 2. The study revealed that the prepared ***P*** showed maximum sensitivity and selectivity in aqueous medium as compared to the previously reported work. ***P*** is an efficient fluorescence ligand in terms of sensitivity, selectivity, and ease of reusability for practical application to remediate toxic $Ni^{2+}$ ions from water samples.

## 4. CONCLUSIONS

A simple synthetic protocol for the synthesis of ***P*** via a condensation reaction has been carried out. Due to the



https://doi.org/10.1021/acsomega.3c03131
ACS Omega 2023, 8, 27500−27509

Table 2. Comparison of the *P* Sensor with Other Fluorescence-Based Organic Sensors for $Ni^{2+}$ Detection in Aqueous Media

| optical probe | LOD | LOQ | references |
|---|---|---|---|
| benzylhydrazone derivative | $7.3 \times 10^{-10}$ | $2.19 \times 10^{-11}$ | 30 |
| pyrimidine-based ligand | $8.9 \times 10^{-9}$ | $2.67 \times 10^{-10}$ | 31 |
| hydrazide derivative | $2.0 \times 10^{-7}$ | $6.0 \times 10^{-7}$ | 32 |
| quantum dots | $0.1 \times 10^{-7}$ | $0.3 \times 10^{-7}$ | 33 |
| quinoline-based sensor | $1.46 \times 10^{-6}$ | $4.38 \times 10^{-6}$ | 34 |
| APAI | $0.46 \times 10^{-7}$ | $1.38 \times 10^{-7}$ | 35 |
| MOFs | $0.46 \times 10^{-6}$ | $1.38 \times 10^{-6}$ | 36 |
| benzothiazole | $7.4 \times 10^{-9}$ | $2.22 \times 10^{-10}$ | 37 |
| Si-NPs | $1.73 \times 10^{-6}$ | $5.19 \times 10^{-6}$ | 38 |
| schiff base ligand | $7.4 \times 10^{-7}$ | $2.22 \times 10^{-8}$ | 39 |
| QDs | $0.1 \times 10^{-6}$ | $0.3 \times 10^{-6}$ | 40 |
| probe P | $2 \times 10^{-10}$ | $6 \times 10^{-10}$ | this work |

presence of the carbonyl oxygen group in ***P***, good photostability and enhanced fluorescence in aqueous medium were displayed by ***P*** upon formation of the $Ni^{2+}$ complex. Job's plot analysis and DFT calculations supported the 2:1 complex formation between ***P*** and $Ni^{2+}$. The ***P*** proved to be an efficient fluorescent probe for the selective sensing of toxic $Ni^{2+}$ ions by the process of fluorescence enhancement among the many other heavy metals chosen with a lower LOD of $2 \times 10^{-10}$ M. Also, ***P*** displayed good reusability with EDTA as a chelating agent. The developed ***P*** proved to be an efficient and time-saving sensor, which put forward the latest trend in the removal of $Ni^{2+}$ ions from water very selectively and economically.

## ■ ASSOCIATED CONTENT

### Data Availability Statement

All concerned data are given in this manuscript.

### Supporting Information

The Supporting Information is available free of charge at https://pubs.acs.org/doi/10.1021/acsomega.3c03131.

Data of probe ***P*** and its $Ni^{2+}$ complex (PDF)

## ■ AUTHOR INFORMATION


### Corresponding Author

**Muhammad Zahoor** − *Department of Biochemistry, University of Malakand, Chakdara 18800 Khyber Pakhtunkhwa, Pakistan;* orcid.org/0000-0002-4528-8517; Email: mohammadzahoorus@yahoo.com

### Authors

**Maria Sadia** − *Department of Chemistry, University of Malakand, Chakdara 18800 Khyber Pakhtunkhwa, Pakistan*

**Jehangir Khan** − *Department of Chemistry, University of Malakand, Chakdara 18800 Khyber Pakhtunkhwa, Pakistan*

**Rizwan Khan** − *Department of Electrical Engineering, Kwangwoon University, Seoul 54047, South Korea*

**Syed Wadood Ali Shah** − *Department of Pharmacy, University of Malakand, Chakdara 18800 Khyber Pakhtunkhwa, Pakistan*

**Adil Zada** − *Department of Chemistry, University of Malakand, Chakdara 18800 Khyber Pakhtunkhwa, Pakistan*

**Riaz Ullah** − *Department of Pharmacognosy, College of Pharmacy, King Saud University, Riyadh 11451, Saudi Arabia;* orcid.org/0000-0002-2860-467X

**Essam A. Ali** − *Department of Pharmaceutical Chemistry, College of Pharmacy King Saud University, Riyadh 11451, Saudi Arabia*

Complete contact information is available at: https://pubs.acs.org/10.1021/acsomega.3c03131


### Author Contributions

M.S.: methodology, visualization, conceptualization, supervision, and writing—original manuscript. J.K.: methodology, investigation, visualization, investigation, and writing—original draft. R.K.: writing, review, and editing. S.W.A.S.: visualization and validation. A.Z.: visualization and software. M.Z.: conceptualization and writing—original draft. R.U. and E.A.A.: methodology, investigation, visualization, investigation, and resources

### Notes

All authors declare that the described work is original.
The authors declare no competing financial interest.
This study does not violate any ethical rules.
All authors have read and approved the manuscript.
All authors have highly agreed to submit this work for publication.

## ■ ACKNOWLEDGMENTS

The authors extend their appreciation to the researchers supporting Project Number (RSP2023R110) King Saud University, Riyadh, Saudi Arabia, for financial support.

## ■ REFERENCES


(1) Teng, Y.; Yang, J.; Zuo, R.; Wang, J. Impact of urbanization and industrialization upon surface water quality: A pilot study of Panzhihua mining town. *J. Earth Sci.* **2011**, *22*, 658.

(2) Manisalidis, I.; Stavropoulou, E.; Stavropoulos, A.; Bezirtzoglou, E. Environmental and Health Impacts of Air Pollution: A Review. *Front. Public Health* **2020**, *8*, No. 14.

(3) Briffa, J.; Sinagra, E.; Blundell, R. Heavy metal pollution in the environment and their toxicological effects on humans. *Heliyon* **2020**, *6*, No. e04691.

(4) Kinuthia, G. K.; Ngure, V.; Beti, D.; Lugalia, R.; Wangila, A.; Kamau, L. Levels of heavy metals in wastewater and soil samples from open drainage channels in Nairobi, Kenya: community health implication. *Sci. Rep.* **2020**, *10*, No. 8434.

(5) Adhikari, S.; Yanuar, E.; Ng, D.-Q. Widespread nickel contamination in drinking water supplies of elementary schools in Taichung, Taiwan. *Environ. Sci. Pollut. Res.* **2022**, *29*, 12531−12539.

(6) Alabsi, B. I.; AL-Hamadi, M. M.; Alwesabi, A. S. Preconcentration of trace nickel lons from aqueous solutions by using a new and low cost chelating polystyrene adsorbent. *Arab. J. Chem.* **2020**, *13*, 6986−6994.

(7) Karimi, M. A.; Kafi, M. Removal, preconcentration and determination of Ni(II) from different environmental samples using modified magnetite nanoparticles prior to flame atomic absorption spectrometry. *Arab. J. Chem.* **2015**, *8*, 812−820.

(8) Talebi, A.; Teng, T. T.; Alkarkhi, A.F.M.; Norli, I.; Low, L. W. Optimization of nickel removal using liquid−liquid extraction and response surface methodology. *Desalin. Water Treat.* **2012**, *47*, 334−340.

(9) Chen, Q.; Yao, Y.; Li, X.; Lu, J.; Zhou, J.; Huang, Z. Comparison of heavy metal removals from aqueous solutions by chemical precipitation and characteristics of precipitates. *J. Water Process Eng.* **2018**, *26*, 289−300.

(10) Kumari, C.; Varughese, B.; Ramji, S.; Kapoor, S. Liquid−Liquid Extraction and Solid Phase Extraction for Urinary Organic Acids: A Comparative Study from a Resource Constraint Setting. *Ind. J. Clin. Biochem.* **2016**, *31*, 414−422.

(11) Karasiński, J.; Tupys, A.; Halicz, L.; Bulska, E. A Novel Approach for the Determination of the Ge Isotope Ratio Using Liquid−Liquid Extraction and Hydride Generation by Multicollector Inductively Coupled Plasma Mass Spectrometry. *Anal. Chem.* **2021**, *93*, 13548−13554.
(12) AliAkbari, R.; Marfavi, Y.; Kowsari, E.; Ramakrishna, S. Recent Studies on Ionic Liquids in Metal Recovery from E-Waste and Secondary Sources by Liquid-Liquid Extraction and Electrodeposition: a Review. *Mater. Circ. Econ.* **2020**, *2*, 10.
(13) Shah, M. T.; Balouch, A.; Alveroglu, E. Sensitive fluorescence detection of Ni2+ ions using fluorescein functionalized Fe3O4 nanoparticles. *J. Mater. Chem. C* **2018**, *6*, 1105−1115.
(14) Dodani, S. C.; He, Q.; Chang, C. J. A Turn-On Fluorescent Sensor for Detecting Nickel in Living Cells. *J. Am. Chem. Soc.* **2009**, *131*, 18020−18021.
(15) Goswami, S.; Chakraborty, S.; Adak, M. K.; Halder, S.; Quah, C. K.; Fun, H.-K.; Pakhira, B.; Sarkar, S. A highly selective ratiometric chemosensor for Ni2+ in a quinoxaline matrix. *New J. Chem.* **2014**, *38*, 6230−6235.
(16) Sarkar, D.; Pramanik, A. K.; Mondal, T. K. Benzimidazole based ratiometric and colourimetric chemosensor for Ni(II). *Spectrochim. Acta, Part A* **2016**, *153*, 397−401.
(17) Prabhu, J.; Velmurugan, K.; Raman, A.; Duraipandy, N.; Kiran, M. S.; Easwaramoorthi, S.; Nandhakumar, R. A simple chalcone based ratiometric chemosensor for sensitive and selective detection of Nickel ion and its imaging in live cells. *Sens. Actuators, B* **2017**, *238*, 306−317.
(18) Chowdhury, B.; Karar, M.; Paul, S.; Joshi, M.; Choudhury, A. R.; Biswas, B. Salen Type Ligand as a Selective and Sensitive Nickel(II) ion Chemosensor: A Combined Investigation with Experimental and Theoretical Modelling. *Sens. Actuators, B* **2018**, *276*, 560−566.
(19) Santhi, S.; Amala, S.; Renganathan, R.; Subhashini, M.; Basheer, S. M. Colorimetric and fluorescent sensors for the detection of Co(II), Ni(II) and Cu(II) in aqueous methanol solution. *Res. Chem. Intermed.* **2019**, *45*, 4813−4828.
(20) Rosiak, D.; Okuniewski, A.; Chojnacki, J. Novel complexes possessing Hg−(Cl, Br, I)···OC halogen bonding and unusual Hg2S2(Br/I)4 kernel. The usefulness of $\tau 4'$ structural parameter. *Polyhedron* **2018**, *146*, 35−41.
(21) Dong, Y.; Fan, R.; Chen, W.; Wang, P.; Yang, Y. A simple quinolone Schiff-base containing CHEF based fluorescence 'turn-on' chemosensor for distinguishing Zn2+ and Hg2+ with high sensitivity, selectivity and reversibility. *Dalton Trans.* **2017**, *46*, 6769−6775.
(22) Lamiel-Garcia, O.; Ko, K. C.; Lee, J. Y.; Bromley, S. T.; Illas, F. When Anatase Nanoparticles Become Bulklike: Properties of Realistic TiO2 Nanoparticles in the 1−6 nm Size Range from All Electron Relativistic Density Functional Theory Based Calculations. *J. Chem. Theory Comput.* **2017**, *13*, 1785−1793.
(23) Khan, A. A.; Esrafili, M. D.; Ahmad, A.; Hull, E.; Ahmad, R.; Jan, S. U.; Ahmad, I. A computational study on the characteristics of open-shell H-bonding interaction between carbamic acid (NH2COOH) and HO2, HOS or HSO radicals. *J. Mol. Model.* **2019**, *25*, 189.
(24) Ahmad, R.; Ali, Z.; Khan, A. A.; Rehman, N. U. Terbium extraction by functionalized surface: experimental and DFT approach. *Adsorption* **2020**, *26*, 117−125.
(25) Sallum, L. O.; Duarte, V. S.; Custodio, J.M.F.; Faria, E.C.M.; da Silva, A. M.; Lima, R. S.; Camargo, A. J.; Napolitano, H. B. Cyclohexanone-Based Chalcones as Alternatives for Fuel Additives. *ACS Omega* **2022**, *7*, 11871−11886.
(26) Zhang, Y.; Zhao, Y.; Zhou, A.; Qu, Q.; Zhang, X.; Song, B.; Liu, K.; Xiong, R.; Huang, C. "Turn-on" ratiometric fluorescent probe: Naked-eye detection of acidic pH and citric acid (CA) by using fluorescence spectrum and its application in real food samples and zebrafish. *Spectrochim. Acta, Part A* **2021**, *261*, No. 120014.
(27) Zhang, B.; Jia, L.; Tian, M.; Ning, N.; Zhang, L.; Wang, W. Surface and interface modification of aramid fiber and its reinforcement for polymer composites: A review. *Eur. Polym. J.* **2021**, *147*, No. 110352.
(28) Khan, A. A.; Ahmad, R.; Ahmad, I. Density functional theory study of emerging pollutants removal from water by covalent triazine based framework. *J. Mol. Liq.* **2020**, *309*, No. 113008.
(29) Su, Y.; Li, H.; Ma, H.; Robertson, J.; Nathan, A. Controlling Surface Termination and Facet Orientation in Cu2O Nanoparticles for High Photocatalytic Activity: A Combined Experimental and Density Functional Theory Study. *ACS Appl. Mater. Interfaces* **2017**, *9*, 8100−8106.
(30) Chandra, R.; Ghorai, A.; Patra, G. K. A simple benzildihydrazone derived colorimetric and fluorescent 'on−off-on' sensor for sequential detection of copper(II) and cyanide ions in aqueous solution. *Sens. Actuators, B* **2018**, *255*, 701−711.
(31) Gu, Y.-Q.; Shen, W.-Y.; Mi, Y.; Jing, Y.-F.; Yuan, J.-M.; Yu, P.; Zhu, X.-M.; Hu, F.-L. Dual-response detection of Ni2+ and Cu2+ ions by a pyrazolopyrimidine-based fluorescent sensor and the application of this sensor in bioimaging. *RSC Adv.* **2019**, *9*, 35671−35676.
(32) Liu, M.; Yin, Z.; Tan, Y.; Li, J.; Peng, H.; Duan, A.; Luo, C. A new acylhydrazine N'-(1,3 dimethylbutylene)-3-hydroxy-naphthohydrazide based fluorescent sensor for the detection of $Ni^{2+}$. *Dyes Pigm.* **2020**, *181*, No. 108582.
(33) Liu, J.; Zhang, Q.; Xue, W.; Zhang, H.; Bai, Y.; Wu, L.; Zhai, Z.; Jin, G. Fluorescence Characteristics of Aqueous Synthesized Tin Oxide Quantum Dots for the Detection of Heavy Metal Ions in Contaminated Water. *Nanomaterials* **2019**, *9*, No. 1294.
(34) Loya, M.; Hazarika, S. I.; Pahari, P.; Atta, A. K. Fluorometric detection of Cu2+ and Ni2+ by a quinoline-based glucopyranose derivative via the excimer of quinoline subunit. *J. Mol. Struct.* **2021**, *1241*, No. 130634.
(35) Jone Celestina, J.; Tharmaraj, P.; Sheela, C. D.; Alphonse, L.; Shakina, J. One-pot green synthesis of optical fluorescent sensor for selective detection of Ni2+ ions and hydro gel studies. *Opt. Mater.* **2020**, *109*, No. 110444.
(36) Qin, B.; Zhang, X.; Zhang, J. A New Multifunctional Zinc−Organic Framework with Rare Interpenetrated Tripillared Bilayers as a Luminescent Probe for Detecting Ni2+ and PO43− in Water. *Cryst. Growth Des.* **2020**, *20*, 5120−5128.
(37) Bai, C.-B.; Liu, X.-Y.; Zhang, J.; Qiao, R.; Dang, K.; Wang, C.; Wei, B.; Zhang, L.; Chen, S.-S. Using Smartphone APP To Determine the CN− Concentration Quantitatively in Tap Water: Synthesis of the Naked-Eye Colorimetric Chemosensor for CN− and Ni2+ Based on Benzothiazole. *ACS Omega* **2020**, *5*, 2488−2494.
(38) Wen, Q.; Jiang, C.; Liu, W.; Zeng, Z.; Gao, J.; Zheng, Y. Fluorescence Determination of Ni2+ Ions Based on a Novel Nano-Platform Derived from Silicon Quantum Dots. *Silicon* **2022**, *14*, 385−392.
(39) Sahu, M.; Manna, A. K.; Chowdhury, S.; Patra, G. K. A novel dihydro phenylquinazolinone-based two-in-one colourimetric chemosensor for nickel(II), copper(II) and its copper complex for the fluorescent colourimetric nanomolar detection of the cyanide anion. *RSC Adv.* **2020**, *10*, 44860−44875.
(40) Kurshanov, D. A.; Khavlyuk, P. D.; Baranov, M. A.; Dubavik, A.; Rybin, A. V.; Fedorov, A. V.; Baranov, A. V. Magneto-Fluorescent Hybrid Sensor CaCO3-Fe3O4-AgInS2/ZnS for the Detection of Heavy Metal Ions in Aqueous Media. *Materials* **2020**, *13*, 4373.


https://doi.org/10.1021/acsomega.3c03131
*ACS Omega* 2023, 8, 27500−27509